Assessing the Predictability of Heavy Rainfall Events in Japan in Early July 2018 on Medium-Range Timescales

Takumi Matsunobu[1] and Mio Matsueda[2]
[1]*Graduate School of Life and Environmental Sciences, University of Tsukuba, Tsukuba, Japan*
[2]*Center for Computational Sciences, University of Tsukuba, Tsukuba, Japan*

Abstract

Extremely heavy rainfall events occurred over western Japan in early July 2018. This study assesses the predictability of these events for the period 5−7 July using three operational medium-range ensemble forecasts available from the European Centre for Medium-range Weather Forecasts (ECMWF), the Japan Meteorological Agency (JMA), and the National Centers for Environmental Prediction (NCEP), and ensemble simulations conducted with an ECMWF model and NCEP operational ensemble initial conditions. All three operational ensembles predicted extreme rainfall on 5−6 July at lead times of ≤ 6 days, indicating the high predictability of this event. However, the extreme rainfall event of 6−7 July was less predictable. The NCEP forecasts, initialised on 30 June, performed better at predicting this event than the other operational forecasts. The JMA forecasts initialised on 1 July showed improved predictability; however, the ECMWF forecasts initialised after 30 June showed only gradual improvements as the initialisation time progressed. The ensemble simulations revealed that the lower predictability of the rainfall in the ECMWF forecasts on 6−7 July can be attributed to the model rather than to the initial conditions. Accurate prediction of the North Pacific Subtropical High is a prerequisite for accurate prediction of such extreme rainfall events.

(**Citation**: Matsunobu, T., and M. Matsueda, 2019: Assessing the predictability of heavy rainfall events in Japan in early July 2018 on medium-range timescales. *SOLA*, **15A**, 19−24, doi: 10.2151/sola.15A-004.)

1. Introduction

Western Japan and Hokkaido experienced severe heavy rains from 28 June to 8 July 2018. The rainfall over western Japan was most severe between 4 and 7 July, which caused many rivers to flood and killed more than 200 people. The cause of this heavy rainfall is thought to be the convergence of water vapour fluxes over the western part of the main island of Japan (JMA 2018). The well-developed North Pacific Subtropical High (NPSH) and the northern ridge of high pressure sandwiched the Japanese islands, channelling the moist air from the southern tropical region to the sandwiched region of western Japan. This synoptic-scale backgrounds were unique and unusual conditions. (Tsuguchi et al. 2019). This suggests that an accurate prediction of synoptic-scale fields at medium-range timescales as well as that of meso-scale fields at short-range timescales can contribute to comprehensive prediction of the heavy rainfall in multi time ranges.

Ensemble prediction systems (EPS) are a major component of recent numerical weather prediction (NWP) in many national weather forecasting centres. Using many perturbed initial/boundary conditions, ensemble forecasts can produce many possible future scenarios and quantify the forecast uncertainties. Operational ensemble forecast data have become accessible due to recent progress in computing power or computational sciences and international research projects organised by the World Meteorological Organisation (WMO) (e.g., The Interactive Grand Global Ensemble (TIGGE; Swinbank et al. 2016) and the Subseasonal to Seasonal (S2S; Vitart et al. 2017) projects). The use of operational ensemble forecast data is an effective way to rapidly respond to severe weather events. A large number of studies have investigated the predictability of atmospheric phenomena using operational ensemble forecast data (e.g., Froude 2010; Gray et al. 2014; Matsueda 2009; 2011; Matsueda and Endo 2011; Matsueda and Nakazawa 2015; Matsueda and Kyouda 2016; Matsueda and Palmer 2018; Yamagami et al. 2018; Yamaguchi and Majumdar 2010; Yamaguchi et al. 2015).

In this study, we investigate the predictability of the rainfall events using operational medium-range ensemble forecasts from the European Centre for Medium-Range Weather Forecasts (ECMWF), the Japan Meteorological Agency (JMA), and the U.S. National Centers for Environmental Prediction (NCEP). We then conduct ensemble simulations using the ECMWF OpenIFS model and NCEP ensemble initial conditions to evaluate the contributions of the model and initial conditions to the forecast of rainfall events.

2. Data and method

2.1 Data

In the present study we analysed the medium-range ensemble forecasts routinely operated at three operational NWP centres: ECMWF (Buizza et al. 2007), JMA (JMA 2007) and NCEP (Zhou et al. 2017) (Table 1). The forecast data are available at the TIGGE (Swinbank et al., 2016) data portal at ECMWF.

The ECMWF ReAnalysis (ERA)-Interim (Dee et al. 2011) data were used as observations for mean sea level pressure (SLP), specific humidity and zonal and meridional winds at 850 hPa. The Global Satellite Mapping of Precipitation (GSMaP; Aonashi et al. 2009) data were also used as observed precipitation. All the forecast and observed data were interpolated onto a common latitude–longitude grid with a spatial resolution of 1.25 degree.

2.2 Probabilistic forecasts based on model climatology

Individual NWP models tend to generate different predictions of atmospheric phenomena, leading to different model climatologies (Matsueda and Nakazawa 2015). Following Matsueda and Nakazawa (2015), the present study defines the forecast probability of severe rainfall based on the climatological probability density functions (PDFs) of each model (Fig. S1 in Supplement). The PDFs for each model and GSMaP were estimated with a 31-day time window at each grid point, each calendar day and each forecast lead time, using the forecast data for each model and GSMaP during June and July of 2006−2011. Note that the model climatologies might have changed with upgrades at each centre after 2011, but that the changes might mainly affect rainfall intensity rather than its spatial distribution. The forecast probability is defined as the fraction of ensemble members that predict a higher value than a specified climatological percentile in each model to ensemble size. The use of the model climatological PDF can remove model biases in probabilistic forecasts and therefore enables us to make fair comparisons of probabilistic forecasts. The observed severe rainfall can be also defined with the corresponding PDF.

Corresponding author: Mio Matsueda, Center for Computational Sciences, University of Tsukuba, 1-1-1 Tennoudai, Tsukuba, Ibaraki, 305-8577, Japan. E-mail: mio@ccs.tsukuba.ac.jp.

Table 1. Summary of operational medium-range ensemble forecast systems as of June 2018.

NWP centre	Forecast model resolution (forecast range)	Initial perturbation method	Model perturbation method	Ensemble size/run
ECMWF	T639L91 (0–240 hours) T319L91 (240–360 hours)	Singular vector	Stochastically Perturbed Physics Tendencies scheme Stochastic Kinetic Energy Backscatter scheme	51
JMA	T479L60 (0–264 hours)	Singular vector	Stochastically Perturbed Physics Tendencies scheme	27
NCEP	T574L64 (0–192 hours) T382L64 (192–384 hours)	Ensemble Kalman Filter	Stochastic Total Tendency Perturbation scheme	21

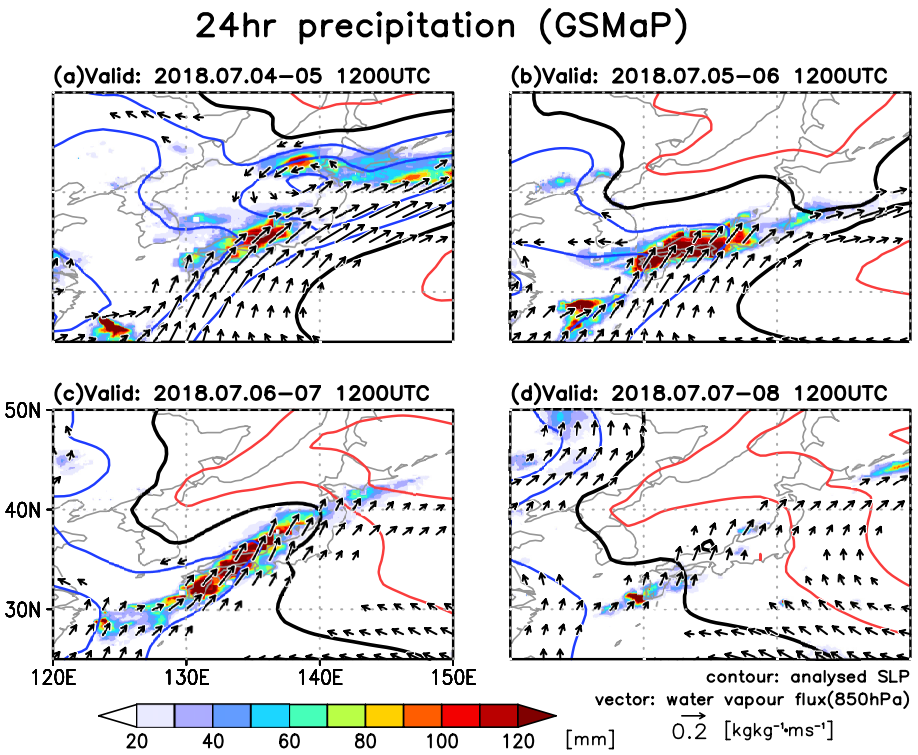

Fig. 1. Observed 24-h precipitation (GSMaP) from 5 to 8 July 2018. Shading shows the accumulated precipitation during the 24 hours up to the valid time. Contours indicate the observed daily mean SLP between (a) 1200 UTC on 4 July and 1200 UTC on 5 July, (b) 1200 UTC on 5 July and 1200 UTC on 6 July, (c) 1200 UTC on 6 July and 1200 UTC on 7 July, and (d) 1200 UTC on 7 July and 1200 UTC on 8 July. The thick black contour indicates a SLP of 1012 hPa, and the blue (red) contours show lower (higher) values than 1012 hPa. The contour interval is 4 hPa. The vectors indicate observed water vapour flux at 850 hPa and are given for fluxes > 0.07 [kg/kg*m/s].

2.3 Ensemble simulations with the ECMWF model and NCEP ensemble initial conditions

To distinguish the contributions of numerical models and analyses to forecast, multi-analysis or multi-model experiments have been conducted (Harrison et al. 1999; Mylne et al. 2002; Matsueda et al. 2011). In this study, we conducted ensemble simulations with the ECMWF OpenIFS model and the NCEP GEFS (Global Ensemble Forecasting System) analyses as initial conditions (hereafter OIFS). Since ECMWF and NCEP showed opposite forecast skills for the latter part of this rainfall event (detailed in Section 3), the comparisons between OIFS and NCEP or ECMWF can reveal whether model formulation and/or initial conditions greatly affect the forecast performance in predicting the rainfall event.

The OpenIFS is the easy-to-use version of the ECMWF operational IFS (Integrated Forecasting System). It is expected to provide similar forecast performance to the IFS as it has the same hydrostatic dynamical core, physics parameterization scheme, land surface model, and wave model. Note that this study used OpenIFS version 40r1 (ECMWF 2014a, 2014b), corresponding to the operational IFS used from 19 November 2013 to 11 May 2015, and did not use any model perturbation methods. The NCEP GEFS analyses are used as initial conditions of the operational medium-range ensemble forecast at NCEP. The NCEP ensemble analyses on 31 pressure levels and a uniform 1.0 degree latitude–longitude grid are linearly vertical-interpolated onto 60 hybrid layers and horizontally interpolated onto the T255 reduced Gaussian grid using spherical harmonic regridding, and are then transformed to spectral coefficients using spherical harmonic functions.

3. Results

3.1 Observed rainfall

Figure 1 shows the observed 24-h precipitation (GSMaP) and SLP from ERA-Interim for the period when extreme rainfall events occurred in western Japan (see Fig. S2 for synoptic positions of each pressure system). On 4 to 5 July (Fig. 1a), the Japanese islands experienced relatively low-pressure conditions due to the passage of typhoon Prapiroon and the location of the NPSH to the southeast of Japan. As a result of strong water vapour fluxes along the edge of the NPSH, heavy rainfall was observed from

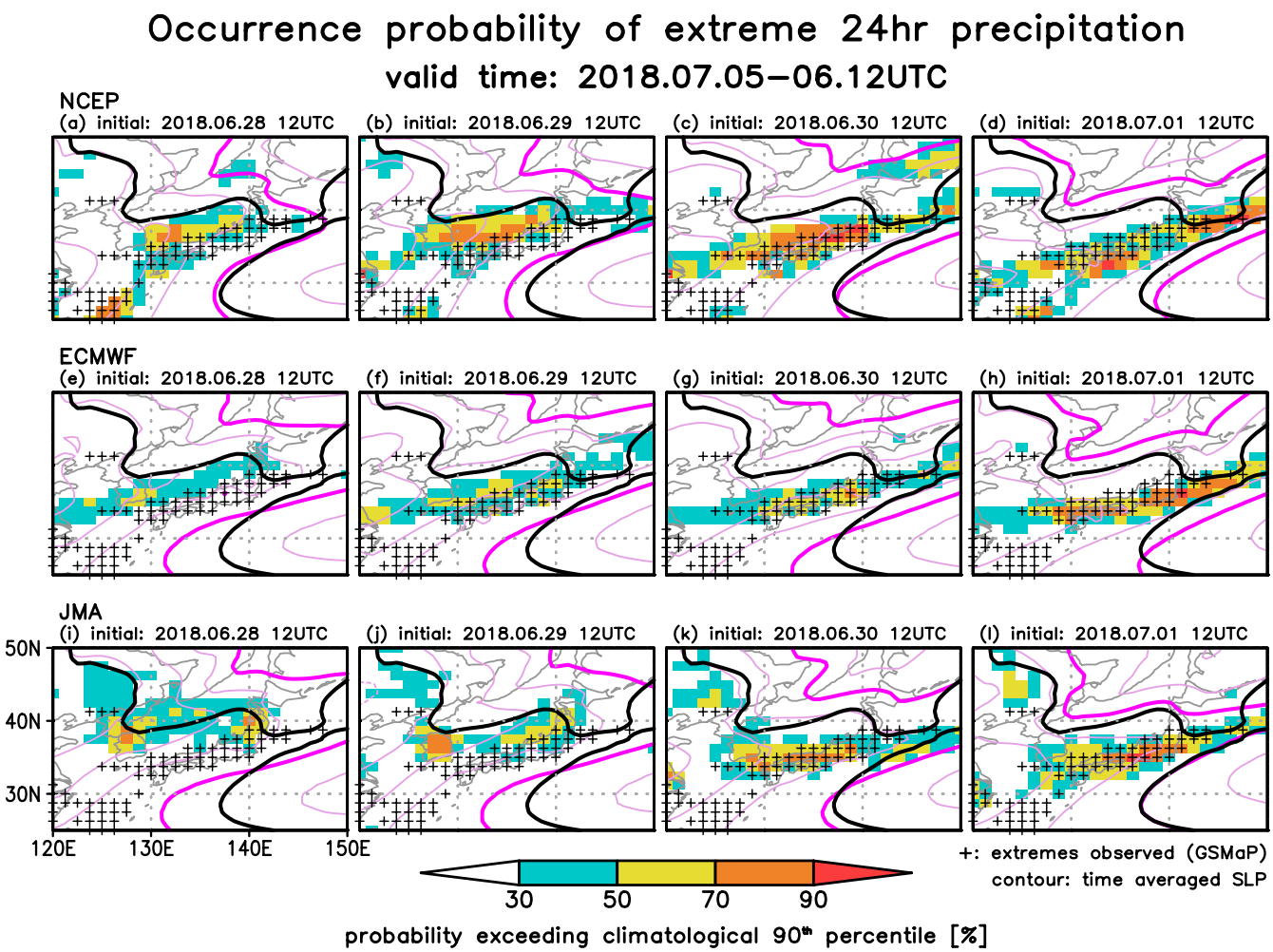

Fig. 2. Occurrence probabilities of severe 24-h precipitation. The shading indicates occurrence probabilities from the (top) NCEP, (middle) ECMWF, and (bottom) JMA ensemble forecasts, initialised at 1200 UTC from 28 June to 1 July 2018, and valid between 1200 UTC on 5 July and 1200 UTC on 6 July 2018. The climatological 90th percentiles of the models were used to define the predicted extremes. The hatching indicates observed extremes defined with the observed climatological 90th percentile. The black and pink contours indicate analysed and predicted ensemble mean SLP of 1012 hPa valid between 1200 UTC on 5 July and 1200 UTC on 6 July 2018, respectively.

the western region of Honshu, Japan's main island, to Shikoku and the northern coast of Kyushu, and over to the eastern Korean Peninsula. The northern ridge of high pressure strengthened and extended southeastward on the following day (Fig. 1b). The NPSH also strengthened. These two ridges of high pressure, located to the north and south of Japan, acted to sandwich Honshu, thus maintaining western Japan under an area of low air pressure (i.e., a depression). Consequently, the rainfall was intensified over this region, as occurred the day before. This was due to the continuous strong southwesterly water vapour fluxes acting along the edge of the NPSH. We refer to this extreme rainfall event, observed between 1200 UTC on 5 July and 1200 UTC on 6 July, as rainfall event one (EVENT1). On 6 to 7 July (Fig. 1c), continuous strong southwesterly water vapour fluxes were observed. The NPSH continued to develop and merged with the strengthened northern high-pressure ridge. The region of rainfall extended from the southwest, off the coast of Kyushu, to east of the Tohoku region, crossing Kyushu, Shikoku and western Honshu. The orientation of the rainband became more southwesterly than that observed on 4−5 and 5−6 July. We refer to this event, occurring between 1200 UTC on 6 July and 1200 UTC on 7 July, as rainfall event two (EVENT2). On 7 to 8 July (Fig. 1d), the low-pressure trough over the Japanese islands showed a weakening trend, leading to reduced southwesterly water vapour fluxes and the subsequent termination of the extreme rainfall event.

3.2 Rainfall predicted by operational ensemble forecasts

The rainfall area of EVENT1 was well predicted 6 days in advance, in forecasts initialised at 1200 UTC on 30 June or later (Figs. 2c, 2d, 2g, 2h, 2k and 2l). Rainfall was predicted farther north than observed in all forecasts initialised at 1200 UTC on 28−29 June (Figs. 2a, 2b, 2e, 2f, 2i and 2j), owing to the modelling of a stronger than observed NPSH and a less-developed ridge of northern high pressure. The ECMWF and NCEP forecasts only partially predicted the extreme rainfall experienced over western Japan, with low (0.3−0.5) and moderate (0.5−0.7) probabilities, respectively. However, the extreme rainfall observed over western Japan (hatching in Fig. 2) was well captured by all ensemble forecasts initialised on and after 30 June (Figs. 2c, 2d, 2g, 2h, 2k and 2l). As the forecast initialisation time progressed, the NPSH was predicted with increasing accuracy, resulting in a more representative ensemble-mean value and improved forecasts capable of capturing the extreme rainfall event. In some cases (Figs. 2d and 2h), the predicted rainfall areas with probability of > 0.3 were extended slightly southwards due to the predicted NPSH being weaker than that observed. The NCEP forecasts tended to predict higher probabilities of severe rainfall than those of the other centres due to their small ensemble spread, as reported in previous studies (e.g., Matsueda and Nakazawa 2015).

All ensemble forecasts predicted EVENT2 (Fig. 3) with less skill than EVENT1 (Fig. 2). All of the forecasts initialised on 29

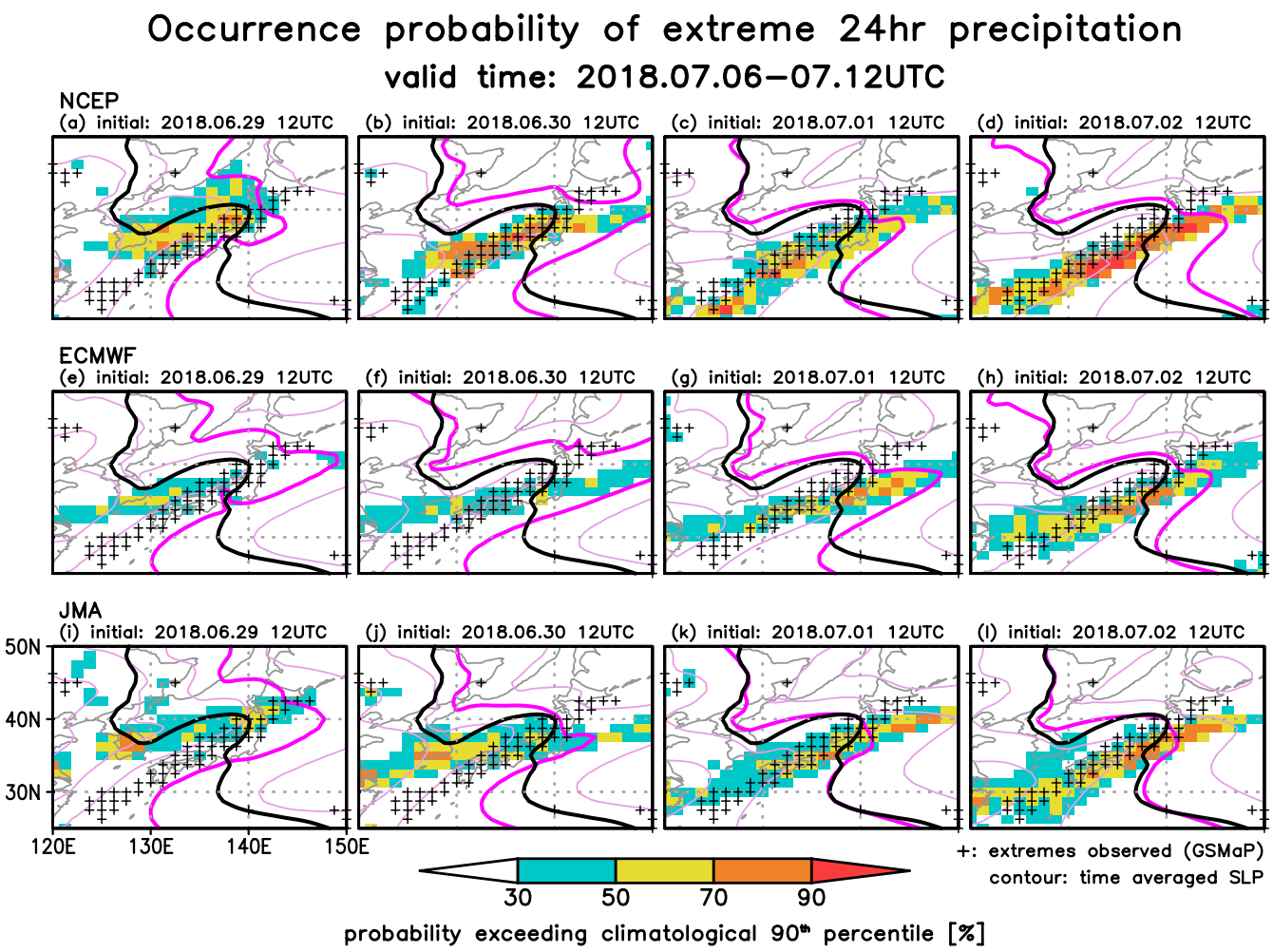

Fig. 3. As for Fig. 2, but initialised at 1200 UTC from 29 June to 2 July 2018 and valid between 1200 UTC on 6 July and 1200 UTC on 7 July 2018.

June (Figs. 3a, 3e, and 3i) predicted extreme rainfall farther north than observed, due to the stronger than observed NPSH and a less-developed ridge of northern high pressure (Figs. 3a, 3e, and 3i). The NCEP forecast initialised on 30 June (Fig. 3b) showed a large improvement in predicting the NPSH and the northern ridge, leading to a substantial improvement in predicting the extreme rainfall, especially over western Japan. The NCEP forecasts initialised on and after 30 June (Figs. 3b, 3c, and 3d) performed best in predicting the rainband characteristics and predicted higher probabilities of occurrence of the heavy rainfall over western Japan than the other centres. The predicted orientations of the rainband tended to be more zonal than observed, especially in the ECMWF forecasts initialised on 30 June and 1 July (Figs. 3f and 3g), and the JMA forecasts initialised on 30 June (Fig. 3j). The JMA forecast initialised on 1 July (Fig. 3k) showed a substantial improvement in predicting the strength of the northern ridge and the NPSH, leading to a substantial improvement in predicting the angle of the rainband. The ECMWF forecast initialised on 30 June (Fig. 3f) resulted in substantial improvement in predicting the northern ridge; however, only a small improvement was observed in prediction of the rainband, suggesting that the orientation of the rainband was mainly attributed to the strength of the NPSH. The ECMWF forecasts initialised on and after 30th June (Figs. 3f and 3g) showed gradual improvement, mainly in predicting the strength of the NPSH, as the forecast initialisation time progressed, resulting in corresponding improvements in predicting the rainband. All forecasts initialised on 2 July (Figs. 3d, 3h, and 3l) captured the general pattern of the observed rainband, but the heavy rainfall to the south of Hokkaido and in northern Tohoku was not predicted, due mainly to the predicted NPSH being weaker than observed. In addition, the ECMWF forecast initialised on 2 July (Fig. 3h) did not predict the extreme rainfall observed over the East China Sea.

Overall, the extreme rainfall observed during EVENT1 was highly predictable 6 days in advance by all three of the centres' ensemble forecast models, whereas only the NCEP model performed well on the same timescale for EVENT2 (See probabilistic verification using Brier Skill Score (Wilks 2011) in Fig. S3). The ECMWF forecasts presented the lowest skill in predicting the rainband during EVENT2. Accurate prediction of the strength of the NPSH was regarded as being more important than that of the northern ridge for the production of improved forecasts of the extreme rainfall observed over western Japan. In the following subsection, the contributions of model formulation and initial conditions to the forecast performance are investigated and distinguished from each other, through an analysis of EVENT2.

3.3 Rainfall predicted by ensemble simulations

The OIFS forecast showed similar characteristics to the operational forecasts (Fig. 4): the predicted strength of the NPSH mainly affected the predicted orientation of the rainband and therefore improvements in this parameter led to improvements in the predicted rainband. The spatial patterns of the rainband predicted by OIFS were comparable with those predicted by ECMWF (Figs. 3e, 3f, 3g, and 3h), whereas the forecast probabilities of extreme rainfall produced by OIFS were more comparable

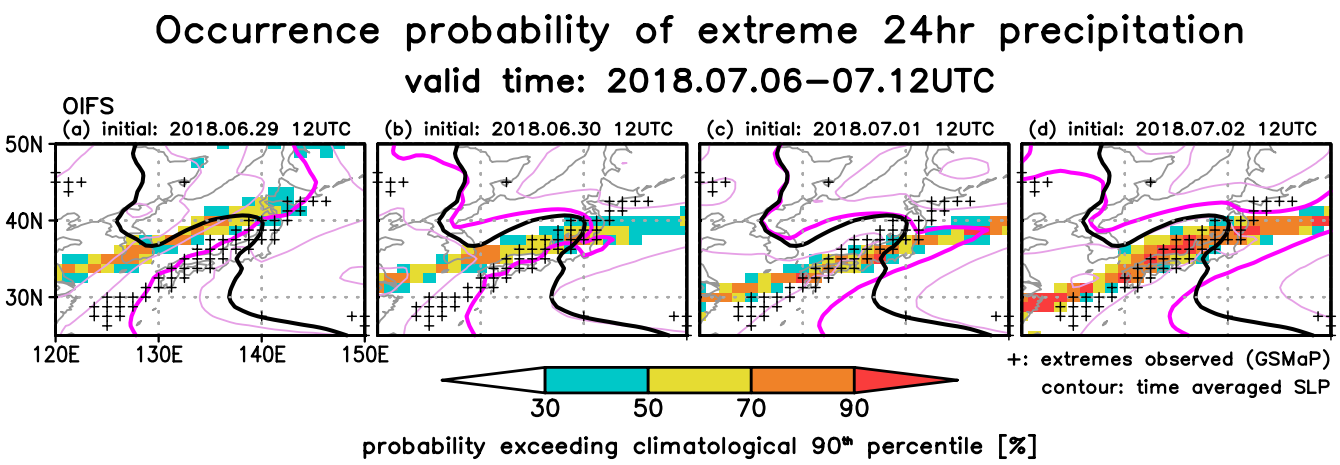

Fig. 4. As in Fig. 3, but for the OIFS simulations.

to those produced by NCEP (Figs. 3a, 3b, 3c, and 3d) and were higher than those of ECMWF. These results suggest that the lower predictability of the rainband location on 6−7 July in the ECMWF forecasts (Figs. 3f, 3g, and 3h) can be attributed mainly to the implementation of the numerical model rather than to the initial conditions. The NCEP initial conditions were found to contribute only to the increase in the occurrence probability of extreme rainfall in the ensemble simulations. The OIFS forecast initialised on 2 July (Fig. 4d) predicted a stronger NPSH and the position of the northern ridge to be slightly more northwards than that observed, resulting in the predicted rainband being shifted far northwards and in a failure to capture the pattern of heavy rainfall over the southwestern part of the observed rainband.

4. Summary

We investigated the predictability of extreme rainfall events in early July 2018 over western Japan using the three operational medium-range ensemble forecasts available from ECMWF, NCEP, and JMA.

The extreme rainfall events occurred between 4 and 7 July 2018. During this period, Honshu, Japan's main island, experienced sustained low-pressure atmospheric conditions as a result of being sandwiched between the NPSH and a ridge of northern high pressure. This led to rainfall intensification over western Japan as a result of continuous strong southwesterly water vapour fluxes that acted along the edge of the NPSH. We focussed on two events: EVENT1, which occurred between 1200 UTC on 5 July and 1200 UTC on 6 July, and EVENT2, which occurred between 1200 UTC on 6 July and 1200 UTC on 7 July. During EVENT1, the extreme rainfall occurred over Western Honshu, Shikoku, and the north coast of Kyushu. During EVENT2, the orientation of the rainband became more southwesterly than during EVENT1 due to the northward development of the NPSH.

Overall, the extreme rainfall observed during EVENT1 was highly predictable 6 days in advance by all three centres, whereas EVENT2 was highly predictable within the same timeframe by only NCEP. The JMA forecasts initialised on 1 July showed a substantial improvement in predicting the rainband during EVENT2, whereas the ECMWF forecasts initialised on and after 30 July showed a gradual improvement as the time of initialisation progressed. The ECMWF forecasts presented the lowest skill in predicting the rainband during EVENT2. Accurate prediction of the strength of the NPSH was more important than that of the northern ridge in producing better forecasts of the extreme rainfall events over western Japan, as well as tropical cyclone landfall for East Asian countries (Camp et al. 2019).

We also conducted ensemble simulations with an ECMWF OpenIFS model, using the NCEP GEFS initial conditions, to distinguish between contributions of the model and the initial conditions to the performance of the forecast in predicting the heavy rainfall observed during EVENT2. The lower predictability of the rainband location on 6−7 July in the ECMWF forecasts is attributed mainly to the model rather than to the initial conditions. The NCEP initial conditions were found to contribute only to the increase in the probability of occurrence of severe rainfall in the ensemble simulations. The higher performance of the NCEP forecasts in predicting EVENT2 was due mainly to the NCEP operational model itself rather than a result of the NCEP GEFS initial conditions.

Further investigation is required to ascertain which physical processes play an important role in achieving accurate model prediction of the strength of the NPSH. It would also be useful to conduct ensemble simulations using an NCEP model and ECMWF initial conditions to assess whether the quality of the ECMWF initial conditions were good enough for an accurate prediction of EVENT2. In addition, it would be interesting to perform further ensemble simulations by swapping the initial perturbations between the ECMWF and NCEP models to assess the impacts of ensemble perturbations on forecast performance. We propose that multi-analysis and multi-model ensemble simulations will become key approaches in clarifying inherent weaknesses in forecasting systems and could therefore contribute to improving the quality of weather predictions and mitigating catastrophic damage resulting from extreme weather events.

Acknowledgement

The authors thank ECMWF for providing ERA-Interim and the THORPEX TIGGE project team for providing the TIGGE data. The authors also thank Japan Aerospace Exploration Agency (JAXA) for providing the GSMaP data. We would like to thank Dr Takeshi Enomoto and Dr Glenn Carver for the OpenIFS support. This work was supported by a Japan Society for the Promotion of Science (JSPS) Grant-in-Aid for Young Scientists (B), Number 16K16378.

Edited by: H. Mukougawa

Supplements

Figure S1 shows the climatological percentiles of 90th precipitation for NWP models.

Figure S2 shows the observed sea level pressure and indicates each pressure system related to the heavy rianfall event.

Figure S3 shows Brier skill scores of EVENT1 and EVENT2 for operational forecasts.

References

Aonashi, K., J. Awaka, M. Hirose, T. Kozu, T. Kubota, G. Liu, S. Shige, S., Kida, S. Seto, N. Takahashi, and Y. N. Takayabu, 2009: GSMaP passive, microwave precipitation retrieval algorithm: Algorithm description and validation. *J. Meteor. Soc. Japan*, **87A**, 119−136.

Buizza, R., J. R. Bidlot, N. Wedi, M. Fuentes, M. Hamrud, G. Holt, and F. Vitart, 2007: The new ECMWF VAREPS (variable resolution ensemble prediction system). *Quart. J. Roy. Meteor. Soc.*, **133**, 681−695.

Camp, J., M. J. Roberts, R. E. Comer, P. Wu, C. MacLachlan, P. E. Bett, N. Golding, R. Toumi, and J. C. L. Chan, 2019: The western Pacific subtropical high and tropical cyclone landfall: Seasonal forecasts using the Met Office GloSea5 system. *Quart. J. Roy. Meteor. Soc.*, **145**, 105−695, doi: 10.1002/qj.3407.

Dee, D. P., and 35 co-authors, 2011: The ERA-Interim reanalysis: Configuration and performance of the data assimilation system. *Quart. J. Roy. Meteor. Soc.*, **137**, 553−597, doi: 10.1002/qj.828.

ECMWF, 2014a: Part III: Dynamics and numerical procedures, *IFS Documentation*, CY40R1. (Available online at https://www.ecmwf.int/sites/default/files/elibrary/2014/9203-part-iii-dynamics-and-numerical-procedures.pdf, accessed 25 March 2019)

ECMWF, 2014b: Part IV: Physical processes, *IFS Documentation*, CY40R1. (Available online at https://www.ecmwf.int/sites/default/files/elibrary/2014/9204-part-iv-physical-processes.pdf, accessed 25 March 2019)

Froude, L. S., 2010: TIGGE: Comparison of the prediction of Northern Hemisphere extratropical cyclones by different ensemble prediction systems. *Wea. Forecasting*, **25**, 819−836, doi:10.1175/2010WAF2222326.1.

Gray, S. L., C. M. Dunning, J. Methven, G. Masato, and J. M. Chagnon, 2014: Systematic model forecast error in Rossby wave structure. *Geophys. Res. Lett.*, **41**, 2979−2987, doi: 10.1002/2014GL059282.

Harrison, M. S. J., T. N. Palmer, D. S. Richardson, and R. Buizza, 1999: Analysis and model dependencies in medium-range ensembles: Two transplant case-studies. *Quart. J. Roy. Meteor. Soc.*, **125**, 2487−2515, doi:10.1002/qj.49712555908.

Japan Meteorological Agency, 2007: *Outline of the operational numerical weather prediction at the Japan Meteorological Agency*. Japan Meteorological Agency, Tokyo.

Japan Meteorological Agency, 2018: *Primary factors behind the heavy rain event of July 2018 and the subsequent heat wave in Japan from mid-July onward*. (Available online at https://ds.data.jma.go.jp/tcc/tcc/news/press_20180822.pdf, accessed 25 March 2019).

Matsueda, M., 2009: Blocking predictability in operational medium-range ensemble forecasts. *SOLA*, **5**, 113−116, doi: 10.2151/sola.2009-029.

Matsueda, M., 2011: Predictability of Euro-Russian blocking in summer of 2010. *Geophys. Res. Lett.*, **38**, L06801, doi: 10.1029/2010GL046557.

Matsueda, M., and H. Endo, 2011: Verification of medium-range MJO forecasts with TIGGE. *Geophys. Res. Lett.*, **38**, L11801, doi:10.1029/2011GL047480.

Matsueda, M., and T. Nakazawa, 2015: Early warning products for severe weather events derived from operational medium-range ensemble forecasts. *Meteorol. Appl.*, **22**, 213−222, doi:10.1002/met.1444.

Matsueda, M., and M. Kyouda, 2016: Wintertime East Asian flow patterns and their predictability on medium-range timescales. *SOLA*, **12**, 121−126, doi:10.2151/sola.2016-027.

Matsueda, M., and T. N. Palmer, 2018: Estimates of flow-dependent predictability of wintertime Euro-Atlantic weather regimes in medium-range forecasts. *Quart. J. Roy. Meteor. Soc.*, **144**, 1012−1027, doi:10.1002/qj.3265.

Matsueda, M., M. Kyouda, Z. Toth, H. L. Tanaka, and T. Tsuyuki, 2011: Predictability of an atmospheric blocking event that occurred on 15 December 2005. *Mon. Wea. Rev.*, **139**, 2455−2470, doi:10.1175/2010MWR3551.1.

Mylne, K. R., R. E. Evans, and R. T. Clark, 2002: Multi-model multi-analysis ensembles in quasi-operational medium-range forecasting. *Quart. J. Roy. Meteor. Soc.*, **128**, 361−384, doi:10.1256/00359000260498923.

Swinbank, R., M. Kyouda, P. Buchanan, L. Froude, T. M. Hamill, T. D. Hewson, J. H. Keller, M. Matsueda, J. Methven, F. Pappenberger, M. Scheuerer, H. A. Titley, L. Wilson, and M. Yamaguchi, 2016: The TIGGE project and its achievements. *Bull. Amer. Meteor. Soc.*, **97**, 49−67. doi:10.1175/BAMS-D-13-00191.1.

Tsuguti, H., N. Seino, H. Kawase, Y. Imada, T. Nakaegawa, and I. Takayabu, 2019: Meteorological overview and mesoscale characteristics of the heavy rain event of July 2018 in Japan. *Landslides*, **16**, 363, doi:10.1007/s10346-018-1098-6.

Vitart, F., and co-authors, 2017: The subseasonal to seasonal (S2S) prediction project database. *Bull. Amer. Meteor. Soc.*, **98**, 163−173, doi:10.1175/BAMS-D-16-0017.1.

Wilks, D., 2011: *Statistical Methods in the Atmospheric Science*. Third, Ed., Academic Press, 704 pp.

Yamagami, A., M. Matsueda, and H. L. Tanaka, 2018: Predictability of the 2012 Great Arctic Cyclone on medium-range timescales. *Polar Sci.*, **15**, 13−23, doi:10.1016/J.POLAR.2018.01.002.

Yamaguchi, M., and S. J. Majumdar, 2010: Using TIGGE data to diagnose initial perturbations and their growth for tropical cyclone ensemble forecasts. *Mon. Wea. Rev.*, **138**, 3634−3655, doi:10.1175/2010MWR3176.1.

Yamaguchi, M., F. Vitart, S. T. K. Lang, L. Magnusson, R. L. Elsberry, G. Elliott, M. Kyouda, and T. Nakazawa, 2015: Global distribution of the skill of tropical cyclone activity forecasts on short- to medium-range time scales. *Wea. Forecasting*, **30**, 1695−1709, doi:10.1175/WAF-D-14-00136.1.

Zhou, X., Y. Zhu, D. Hou, Y. Luo, J. Peng, and R. Wobus, 2017: Performance of the new NCEP Global Ensemble Forecast System in a parallel experiment. *Wea. Forecasting*, **32**, 1989−2004, doi:10.1175/WAF-D-17-0023.1.

Manuscript received 27 March 2019, *accepted 9 May 2019*
SOLA: *https://www.jstage.jst.go.jp/browse/sola/*